6th European Conference on Computational Mechanics (ECCM 6)
7th European Conference on Computational Fluid Dynamics (ECFD 7)
11 – 15 June 2018, Glasgow, UK

EFFECT OF CONSTITUTIVE LAWS USING COHESIVE ELEMENTS ON CRACKS PATTERNS IN CONCRETE AT THE MESO-SCALE

JERZY BOBIŃSKI[1] AND JACEK TEJCHMAN[2]

[1]Gdańsk University of Technology, Faculty of Civil and Environmental Engineering
Gabriela Narutowicza 11/12, 80-233 Gdańsk, Poland
bobin@pg.edu.pl, https://pg.edu.pl

[2] Gdańsk University of Technology, Faculty of Civil and Environmental Engineering
Gabriela Narutowicza 11/12, 80-233 Gdańsk, Poland
tejchmk@pg.edu.pl, https://pg.edu.pl

Key words: Concrete, Cracks, Meso-scale, Cohesive Elements.

Summary. The paper presents results of two-dimensional meso-scale simulations of fracture in notched concrete beams subjected to three-point bending. Concrete heterogeneity was taken into account by considering a 4-phase material description: aggregate, cement matrix, interfacial transitional zones (ITZs) and macro-voids. The particle distribution was taken from real concrete beams on the basis of X-ray μCT scans. Interface cohesive finite elements were applied to simulate cracks at the meso-scale. The effect of different damaged-based isotropic formulations combining tractions and relative displacements on the crack's surface were investigated. The obtained results were compared with the experimental outcomes. A satisfactory agreement with respect to the load-displacement and crack geometry was achieved between FE analyses and experiments.

1 INTRODUCTION

Concrete can be described at several levels. At the macro-scale all material properties are averaged and the attention is paid to cracking. More detailed simulations take the internal structure of concrete into account. When describing concrete at the meso-level: aggregates, cement matrix, macro-voids and interfacial transition zones (ITZs) may be distinguished [1]. All phases have different elastic and strength properties that influence the overall behaviour of concrete specimens. The experiments and numerical simulations evidently show that the concrete fracture behaviour strongly depends on its meso-structure (e.g. aggregate volume, aggregate size, aggregate roughness, aggregate stiffness, particle size distribution curve, mortar volume and macro-porosity).

Concrete fracture is very complex due to the occurrence of phenomena such as: branching, coalescence, kinking, tortuousness and interlocking of cracks. In order to realistically describe concrete fracture, its internal structure should be taken into account at least at the meso-scale. In particular, the aggregate presence is crucial as its volume fraction in concrete may be approximately 70–75%. Since fracture process starts in interfacial transitional zones (ITZs), thus it is crucial to properly determine their properties. ITZs are a porous region of the cement paste around aggregate particles which is perturbed by their presence. Their width is about 0–50 μm depending upon the aggregate roughness.

Within continuum mechanics, there exist two main approaches to describe this process. The first one describes it in a smeared sense as localized zones of micro-cracks with a certain finite width. Continuous constitutive models suffer from the finite element mesh sensitivity and numerical results do not coincide as a mesh is refined. Therefore, the classical models need to be enhanced with a characteristic length of micro-structure in order to tackle the aforementioned numerical problems. This extension can be performed with different theories: micro-polar, strain gradient, viscous and non-local ones. As an alternative, displacement jumps (discontinuities) along cracks may be introduced while keeping the remaining region as a continuous one. It can be achieved by defining interface finite elements placed along element boundaries or using eXtended Finite Element Method. It is also possible to model the concrete behaviour with the use of discrete models which include lattice models or discrete element method (DEM). The description of cracks should also reflect the anisotropy and heterogeneity of concrete.

The mesoscopic approach presented here uses interface cohesive elements to simulate cracks at the mesoscale [2-3]. Numerical models using cohesive elements for modelling fracture do not need to be regularized with the aid of a characteristic length, since a crack or a shear zone is created in a discrete way. For this reason discontinuous approaches are very popular and widely used in fracture studies [4-6]. Unfortunately this approach possesses some drawbacks. The main disadvantage is that cracks paths are dominated by preferred mesh orientations. Crack trajectories are limited to bulk element boundaries and a diffuse cracking pattern is strongly mesh-dependent. The too high initial stiffness of interface elements may lead to traction oscillations in the elastic regime. Both the global (force-displacement curve) and local (crack trajectory/geometry) response of structures becomes mesh-independent when the material heterogeneity is taken into account. The material internal structure is taken into account by considering four different phases, namely aggregate, cement matrix, ITZs and macro-voids. The shapes and positions of aggregates are obtained with the aid of X-ray micro-computed tomography images of real concrete specimens [7]. Different elastic properties are assumed for bulk finite elements covering aggregate grains, cement matrix and homogeneous region. Different fracture properties (critical traction and fracture energy) are chosen for aggregate-cement matrix and cement matrix-cement matrix interfaces. Such a description of concrete eliminates 2 main drawbacks of the use of interface elements to a fracture process: mesh alignment dependency and convergence problems in simulations of curved cracks. A crack nucleates when a crack initiation criterion is fulfilled whereas the post-peak behaviour is governed by a traction-separation law. Crack paths are limited to solid element boundaries. Cracks can be created inside the cement matrix and between aggregates and cement matrix (in ITZs) but no cracks are allowed inside of aggregates. There are not any predefined crack paths.

In the paper the influence of constitutive laws describing fracture on crack patterns was investigated. Different damaged-based isotropic formulations relating tractions and relative displacements on the crack's surface were assumed. Numerical simulations of a three-point bending test were performed. The 2D numerical simulations were carried out with the commercial FE package Abaqus. A complex fracture process was successfully captured by the interface elements equipped with a traction-separation law. The obtained results were compared with the experimental outcomes.

2 EXPERIMENT

Laboratory tests were carried out with two simply-supported concrete beams subjected to three-point bending, denoted in the paper as the beam '1' and beam '2'. The detailed description can be found in [1]. Each specimen had a rectangular cross-section with the height of H=80 mm and width of B=40 mm. The beam length was L=320 mm (4×H) and the span between the supports was 3×H=240 mm. A notch with the height of H/10=8 mm and the width of 3 mm was located in the middle of the bottom edge. The quasi-static beam tests were performed with a constant controlled crack mouth (notch) opening displacement rate (CMOD) using the loading machine Instron 5569. The loading machine feedback was carefully controlled in order to maintain the constant rate of 0.002 mm/min. Each test ended for CMOD = 0.10–0.15 mm prior to the unstable failure in order to provide images of internal meso-structure by means of μCT. Figure 1 presents the geometry and the boundary conditions of the test.

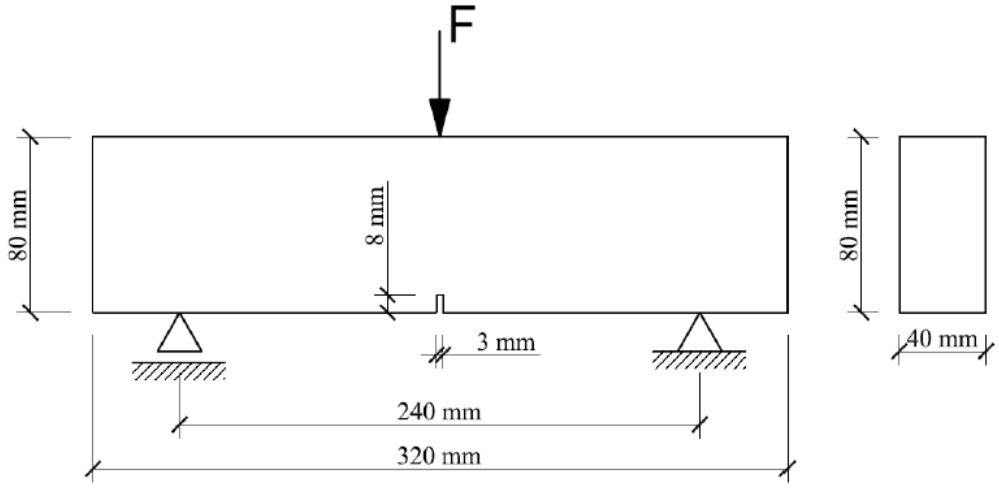

Figure 1: Geometry and boundary conditions

The concrete was composed of aggregate, sand, Portland cement (CEM I 32.5 R) and water. The maximum aggregate diameter was d_{max} = 16 mm and mean particle size was d_{50} = 2.0 mm. The water/cement, sand/cement and aggregate/cement ratios were 0.42, 0.80 and 1.43, respectively. The total aggregate and sand volumetric content was V=75%. Standard curing conditions with the relative humidity greater than 90% and temperature of 20°C were applied to concrete specimens. The average uniaxial compressive strength was equal to f_c=51.81 MPa. The Young modulus E and Poisson's ratio ν were: E=36.1GPa and ν=0.22, respectively. The measured tensile strength during bending on the concrete beams 4×4×16 cm^3 was $f_{t,flex}$=3.7-4.3 MPa (the tensile strength was 3.73–3.91 MPa).

Two experimental diagrams of the vertical force F versus CMOD for the concrete beams (with the displacement CMOD up to 0.15 mm for the beam '1' and up to 0.10 mm for the beam '2') are shown in Fig. 2. The maximum vertical force F was equal to 2.15–2.25 kN. The distribution of aggregate grains and macro-voids in concrete beams was determined based on μCT-images of the concrete cuboids (80×50×40 mm^3) extracted from the mid-part of each

beam after tests. The X-ray micro-tomography system Skyscan 1173 was used to generate 3D images of the concrete meso-structure (Fig. 3). The main discrete macro-crack was strongly curved along the beam height and width due to a random presence of aggregate grains and it propagated mainly through the weakest phase in concrete which were the interfacial transitional zones (ITZs). When two interfacial cracks occurred around adjacent aggregates, a crack inside the cement matrix initiated to bridge the interfacial cracks so that a connected crack path was formed. Sometimes the crack propagated through macro-voids and very rarely through a single weak aggregate grain. For the beam '1', the main crack propagated through the entire specimen's height, whereas it did not reach the top surface in the beam '2'. The scanning electro-microscope (SEM) Hitachi TM3030 was used to measure the width of ITZs. A very non-uniform porous structure of ITZs as well as the presence of separated small sand grains was possible to be observed with the maximum magnification factor of 30,000. The width of porous ITZs did not depend on aggregate particles diameter and changed between 30-50 μm [1].

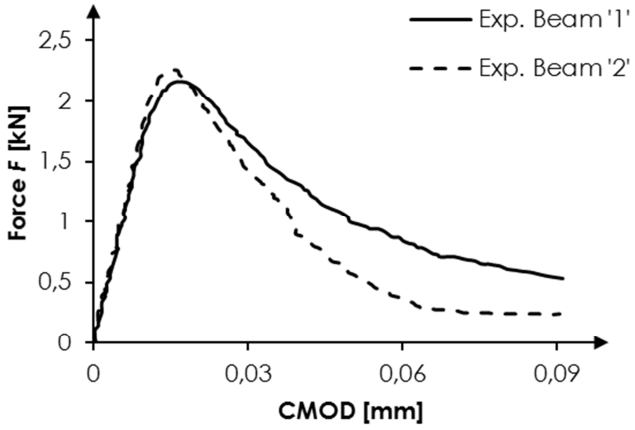

Figure 2: Force-CMOD curves from experiments

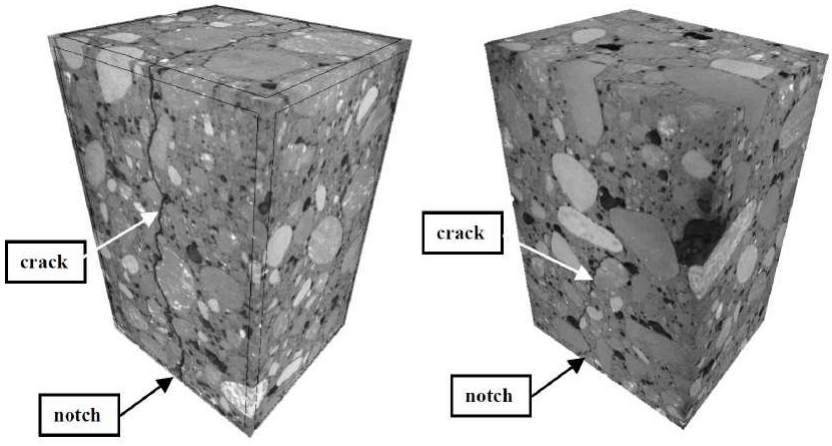

Figure 3: μCT-images of concrete cracked cuboids cut out from beam '1' (left) and '2' (right).

3 CONSTITUTIVE LAWS

The interface finite elements with cohesive traction-separation laws were inserted between solid elements in the beam's mid-region to simulate the cracks nucleation and propagation. Two constitutive laws were defined to describe the behavior of concrete in solid (bulk) and interface finite elements, respectively. Plane stress 3-node triangular elements and 4-node interface elements were used.

3.1 Continuum linear elasticity

An isotropic linear elastic model was assumed for solid elements in the whole specimen throughout the entire analysis. The constitutive matrix $\boldsymbol{C}$ related the stress vector $\boldsymbol{\sigma}$ with the strain vector $\boldsymbol{\varepsilon}$ as:

$$\boldsymbol{\sigma} = \boldsymbol{C}\boldsymbol{\varepsilon} \tag{1}$$

The only required material constants for continuum elements were: Young's modulus E and Poisson's ratio v.

3.2 General traction-relative displacement law

The behaviour of cohesive elements was governed by the following equation:

$$\begin{bmatrix} t_n \\ t_s \end{bmatrix} = \begin{bmatrix} k_n & 0 \\ 0 & k_s \end{bmatrix} \begin{bmatrix} \delta_n \\ \delta_s \end{bmatrix} \tag{2}$$

where t_n and t_s are the tractions, k_n and k_s denote the interface stiffnesses, and δ_n and δ_s are the relative displacements (index 'n' stands for the normal direction while the index 's' describes the tangential direction). Before cracking, the stiffnesses k_n and k_s were equal to the initial (penalty) stiffnesses k_{n0} and k_{s0}, respectively. In all simulations both the stiffnesses were taken as 10^6 MPa/mm for all interface types [6, 8]. The assumed stiffness ensured all cohesive elements to be intact in the elastic deformation range (almost without relative displacements). The selected values were not too large and they did not lead ill-conditioning numerical problems and traction oscillations before cracking. After cracking both the stiffnesses were reduced by the scalar variable D according to:

$$\begin{aligned} k_n &= (1-D)k_{n0} \\ k_s &= (1-D)k_{s0} \end{aligned} \tag{3}$$

3.3 Crack initiation criteria

Two crack initiation criteria were investigated. Both criteria coupled normal and shear tractions in a cohesive element. First, the quadratic nominal stress criterion was assumed:

$$\left\{\frac{\langle t_n \rangle}{t_{n0}}\right\}^2 + \left\{\frac{t_s}{t_{s0}}\right\}^2 = 1 \tag{4}$$

where t_{n0} and t_{s0} are the critical tractions for the fracture mode I and II, respectively, and $\langle\ \rangle$

is the Macaulay bracket. Second, the maximum nominal stress criterion was used:

$$\max\left\{\frac{\langle t_n \rangle}{t_{n0}}, \frac{t_s}{t_{s0}}\right\} = 1 \tag{5}$$

In both criteria the critical traction t_{n0} can be interpreted as the tensile strength.

3.4 Post-peak softening definition

The effective relative displacement δ_m was introduced: to describe damage under a combination of normal and shear deformations across the interface:

$$\delta_m = \sqrt{\langle \delta_n \rangle^2 + \delta_s^2} \tag{6}$$

Note that the sensitivity with the respect to normal and shear terms was excluded here (no scaling coefficient). The exponential softening curve was chosen to describe the behaviour of the interface elements in a post-peak regime. The scalar damage variable D, dependent on the effective relative displacement, was calculated as:

$$D = 1 - \frac{\delta_m^0}{\delta_m^{\max}}\left(1 - \frac{1 - \exp\left(-\alpha\left(\frac{\delta_m^{\max} - \delta_m^0}{\delta_m^f - \delta_m^0}\right)\right)}{1 - \exp(-\alpha)}\right) \tag{7}$$

where δ_m^0 is the effective relative displacement at the crack initiation, δ_m^f is the effective relative displacement at the complete damage, $\delta_m^{\max}$ denotes the maximum effective relative displacement obtained during the loading history and α defines the parameter that affects the slope of the softening curve. Equation (7) was valid only for the displacement smaller than the displacement δ_m^f. If this condition was not fulfilled, the damage parameter D=1 was used.

4 FE SIMULATIONS

4.1 Input data

Numerical simulations were performed in the Abaqus Standard commercial program. Plane stress conditions were assumed. In the beam's mid-region, concrete was described as a heterogeneous material (area 50×80 mm^2) while in the remaining beam part was described as a homogeneous one. Cohesive elements were placed between all bulk elements in the beam's mid-region only. The aggregate and void distributions in the concrete beam were taken into account. The aggregate particles had the diameter 2 mm ≤ da ≤ 16 mm. Their location was the same as on the X-ray μCT images. The macro-voids were simulated as the empty spots. The deformation was induced by enforcing the vertical displacement of nodes at the beam top (under the loading plate with the width of 3.0 mm) up to the final value of 0.2 mm.

In the homogeneous beam's part (wherein the usual 1-phase description was applied), the Young modulus was taken as E_h=36.1 GPa. The Young's modulus of aggregate grains was equal to E_a=47.2 GPa and it was calculated as the weighted average of the moduli of individual components. For the cement matrix the bulk elements the value of E_{cm}=29.2 GPa was chosen. The Poisson's ratio for each material phase was taken as ν=0.22. The shear critical traction t_{s0} for all cohesive elements was assumed to be the same as the normal one ([5, 9]). Different values were assigned to different interface types. For the inter-phase (aggregate/cement matrix), the value $t_{n0,ITZ}$=1.6 MPa was assumed and for the intra-phase (cement matrix/cement matrix), the value $t_{n0,cm}$=4.4 MPa was chosen. No cracks were allowed to create between aggregate solid elements. The displacement at failure δ_m^f was equal to 0.098 mm and 0.071 mm inter-phase (ITZ) and intra-phase (cement matrix) interfaces, respectively. The α parameter was 7.5. These values were chosen in such a way to obtain the fracture energy equal to 20 N/m and 40 N/m for inter-phase and intra-phase interfaces, respectively ([5, 6]). The detailed description of the model parameters can be found in [2, 3].

In general in each beam three different cross-sections at different depths from the front face were analyzed [2] see Fig. 4. In this paper, however, only one section at the depth of 5 mm from the beam '2' was simulated.

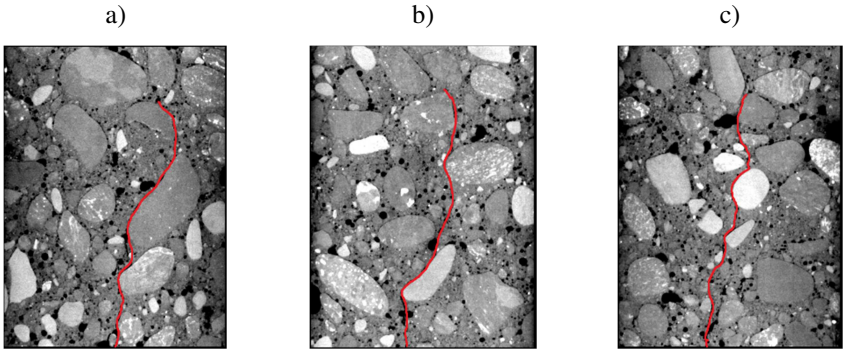

Figure 4: Experimental crack patterns for the beam '2' at the different depths: a) 5 mm, b) 20 mm c) and 35 mm.

4.2 Results with maximum nominal stress criterion

First the influence of critical shear tractions was investigated. Both the critical shear tractions between the cement matrix-cement matrix (4.4 MPa) and cement matrix-aggregates (1.6 MPa, ITZ) were scaled by the factor of 0.5, 2.0 and 5.0. Figure 5 presents the obtained crack patterns. For the smaller factors (0.5 and 1.0), the calculated cracks were similar to the experimental outcomes. The simulations with the higher factors (2.0 and 5.0) resulted in more straight cracks that were not experimentally observed. The calculated force-displacement diagrams are depicted in Fig. 6. The larger the factor was, the higher maximum load was obtained (with the exception of the factor of 5.0).

Next the influence of the critical tractions in the ITZ was examined. Three values of the normal and shear critical tractions were analyzed: 1.6 MPa (base value), 2.2 MPa and 3.3 MPa. Form Fig. 6 it can be seen that the larger value of the critical traction in ITZ was, the more straight crack was obtained. Only simulations with the critical traction equal to 1.6 MPa produced results in agreement to experiments.

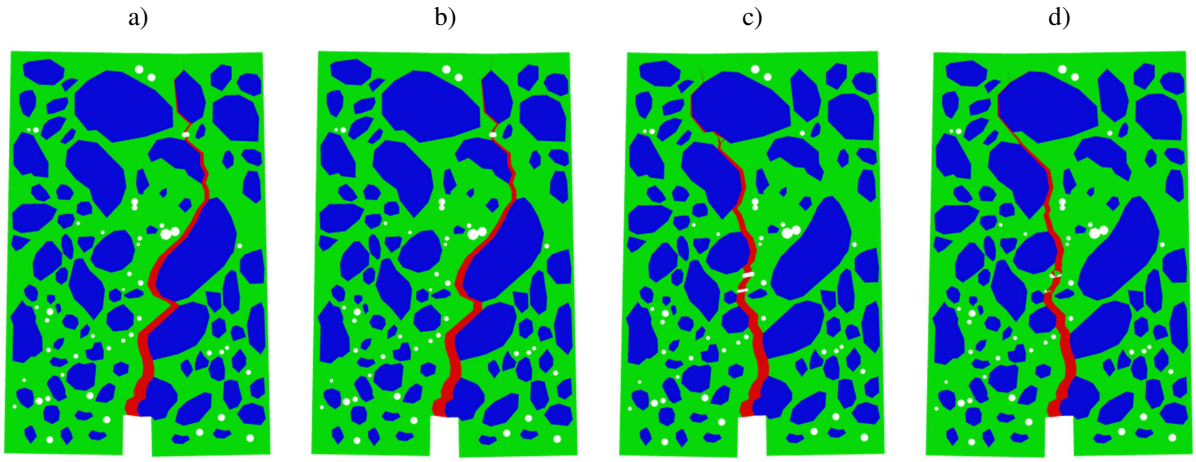

Figure 5: Calculated crack patterns (red colour) for maximum nominal stress criterion and different fractions of shear critical tractions: a) 50%, b) 100%, c) 200% and d) 500% of basis values.

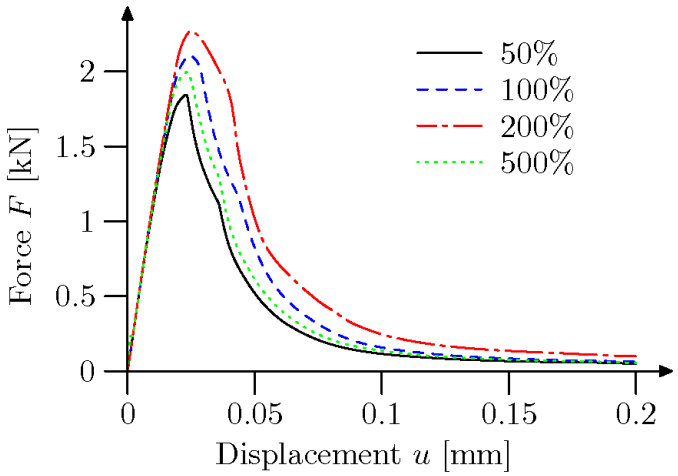

Figure 6: Force-displacement curves for the maximum nominal stress criterion and different fractions of shear critical tractions.

4.3 Results with quadratic nominal stress criterion

First, the influence of the critical shear tractions was investigated. Both the critical shear tractions between the cement matrix-cement matrix (4.4 MPa) and cement matrix-aggregates (1.6 MPa, ITZ) were scaled by the factor of 0.5, 2.0 and 5.0. Figure 8 presents the calculated crack patterns. For the smaller factors (0.5, 1.0 and 2.0), the calculated cracks were similar to the experimental outcomes (some minor discrepancies occurred for the factor 2.0). Only simulations with the highest factors (5.0) resulted in more straight cracks that were not experimentally observed. The calculated force-displacement diagrams are depicted in Fig. 9. The larger the factor was, the higher maximum load was obtained.

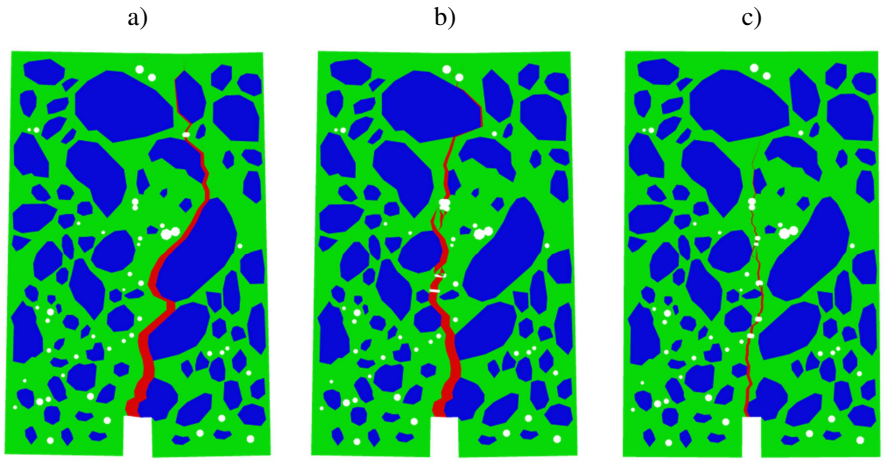

Figure 7: : Calculated crack patterns (red colour) for maximum nominal stress criterion and different critical shear tractions in ITZs: a) 1.6 MPa, b) 2.2 MPa and c) 3.3 MPa.

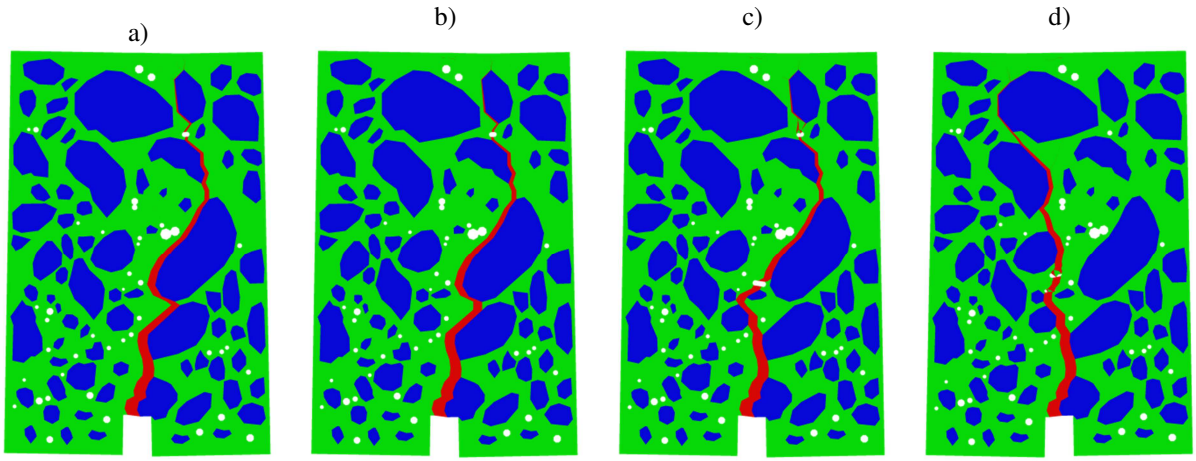

Figure 8: Calculated crack patterns (red colour) for quadratic nominal stress criterion and different fractions of shear critical tractions: a) 50%, b) 100%, c) 200% and d) 500% of basis values.

Next the influence of the critical tractions in ITZs was examined. Three values of the normal and shear critical tractions were analyzed: 1.6 MPa (basis value), 2.2 MPa and 3.3 MPa. Form Fig. 10 it may be seen that the larger the critical traction in ITZs was, the more straight macro-crack was obtained. Only the simulations with the critical traction equal to 1.6 MPa produced results in agreement to experiments.

5 CONCLUSIONS

The numerical calculations showed the ability of cohesive interface elements to reproduce realistic crack patterns at the meso-scale. Two different crack initiation criteria were investigated, but no major differences were observed. The computed crack patterns were influenced by shear critical tractions an critical tractions in ITZs. The higher values resulted in the larger maximum loads, but more straight (non-realistic) macro-cracks.

The current research is focused on simulations with a discrete Mohr-Coulomb criterion. The physical background for the determination of model parameters will be studied.

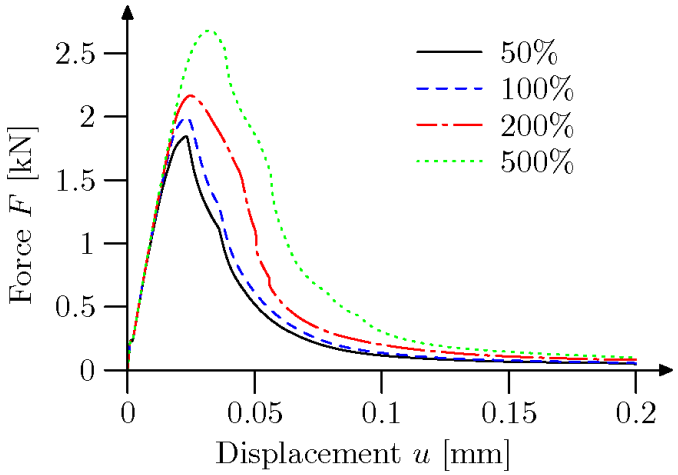

Figure 9: Force-displacement curves for quadratic nominal stress criterion and different fractions of shear critical tractions.

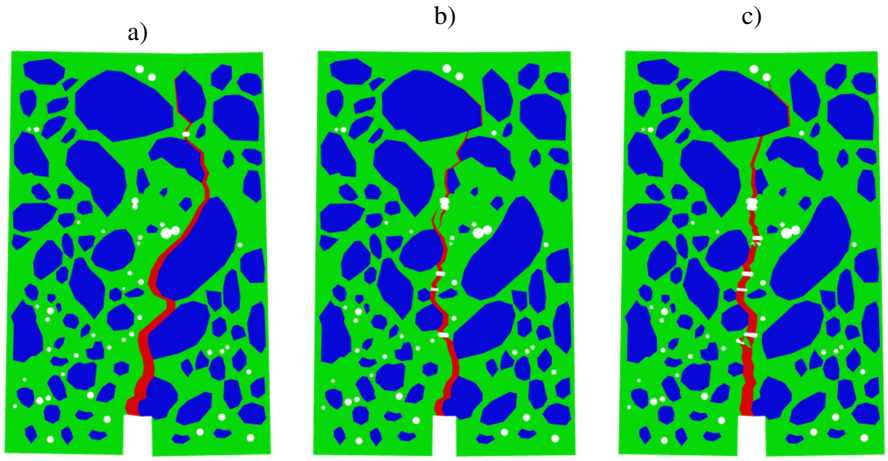

Figure 10: Calculated crack patterns (red colour) for quadratic nominal stress criterion and different critical shear tractions in ITZs: a) 1.6 MPa, b) 2.2 MPa and c) 3.3 MPa.

ACKNOWLEDGEMENTS

The research work has been carried out within the project "Effect of concrete meso-structure on initiation and propagation of cracks - experiments and two-scale numerical model" financed by the Polish National Science Centre (NCN) (UMO-2017/25/B/ST8/02108). The FE calculations were carried out at the Academic Computer Centre in Gdańsk.

REFERENCES

[1] Skarżyński, Ł. and Tejchman, J. Experimental investigations of fracture process in concrete by means of X-ray micro-computed tomography. *Strain* (2016) **52**:26-45.

[2] Trawiński, W., Bobiński, J. and Tejchman, J. Two-dimensional simulations of concrete fracture at aggregate level with cohesive elements based on X-ray μCT images. *Engng.*

Fract. Mech. (2016) **168**:204-26.

[3] Trawiński, W., Tejchman, J. and Bobiński, J. A three-dimensional meso-scale modelling of concrete fracture, based on cohesive elements and X-ray μCT images. *Engng. Fract. Mech.* (2018) **189**:27-50.

[4] Tejchman, J. and Bobiński, J. *Continuous and discontinuous modelling of fracture in concrete using FEM*. Springer, Berlin-Heidelberg, (2013).

[5] Ren, W., Yang, Z., Sharma, R., Zhang, Ch. and Withers, P.J. Two-dimensional X-ray CT image based meso scale fracture modelling of concrete. *Engng. Fract. Mech.* (2015) **133**:24-39.

[6] Wang, X., Zhang, M. and Jivkov, A.P. Computational technology for analysis of 3D meso-structure effects on damage and failure of concrete. *Int. J. Solids Struct.* (2016) **80**:310-333.

[7] Skarżyński, Ł., Nitka, M. and Tejchman, J. Modelling of concrete fracture at aggregate level using FEM and DEM based on X-ray μCT images of internal structure. *Engng. Fract. Mech.* (2015) **147**:13-35.

[8] López, C.M., Carol, I. and Aguado, A. Meso-structural study of concrete fracture using interface elements. I: numerical model and tensile behavior. *Mater. Struct*. (2008) **41**:583-99.

[9] Su, X.T., Yang, Z.J. and Liu, G.H. Monte Carlo simulation of complex cohesive fracture in random heterogeneous quasi-brittle materials: A 3D study. *Int. J. Solids Struct.* (2010) **47**:2336 45.